ADVANCED FUNCTIONAL MATERIALS
www.afm-journal.de

Towards a Better Prediction of Cell Settling on Nanostructure Arrays—Simple Means to Complicated Ends

*Nina Buch-Månson, Sara Bonde, Jessica Bolinsson, Trine Berthing, Jesper Nygård, and Karen L. Martinez**

Vertical arrays of nanostructures (NSs) are emerging as promising platforms for probing and manipulating live mammalian cells. The broad range of applications requires different types of interfaces, but cell settling on NS arrays is not yet fully controlled and understood. Cells are both seen to deform completely into NS arrays and to stay suspended like tiny fakirs, which have hitherto been explained with differences in NS spacing or density. Here, a better understanding of this phenomenon is provided by using a model that takes into account the extreme membrane deformation needed for a cell to settle into a NS array. It is shown that, in addition to the NS density, cell settling depends strongly on the dimensions of the single NS, and that the settling can be predicted for a given NS array geometry. The predictive power of the model is confirmed by experiments and good agreement with cases from the literature. Furthermore, the influence of cell-related parameters is evaluated theoretically and a generic method of tuning cell settling through surface coating is demonstrated experimentally. These findings allow a more rational design of NS arrays for the numerous exciting biological applications where the mode of cell settling is crucial.

1. Introduction

Over the past decade, cell behavior on arrays of vertical nanostructures (NSs) has been the focus of numerous studies aimed at evaluating these as tools for manipulating and probing single cells,[1] in addition to their use as, e.g., highly sensitive protein arrays.[2] Such arrays of high-aspect-ratio NSs have proven to be largely compatible with mammalian cells[3–8] and are currently being established as platforms for a wide variety of advanced applications. Arrays of electrically contacted NSs have been used to locally electroporate and measure action potentials for multiple beating cardiomyocytes in parallel[8,9] or to map individual synaptic connections between primary neurons.[10] Hollow NSs connected with an underlying reservoir have been established as robust platforms for repeatedly introducing otherwise cell-impermeant macromolecules to the cell cytoplasm,[7,11–13] in particular when combined with local administration of detergent or electroporation, and an increased cellular uptake of various molecules has also been reported for some arrays of functionalized solid NSs.[14–18] Flexible NSs can be used to measure and resolve differences in the diminutive forces that cells exert on surfaces,[19,20] and the specific topographical and mechanical environment imposed by a given NS array can be used to fine-tune the fate and behavior of stem cells[21,22] with the prospect of using NS arrays in tissue engineering.

For many of these exciting applications, the mode of cell settling is of utmost importance. For instance, efficient local electroporation at the NS, which is a prerequisite to intracellular electrical measurements, requires a tight interaction along the length of the NS. On the contrary, the use of flexible NSs to sense the traction forces exerted by single cells demands that the cells adhere only to the very tips of the NSs. Furthermore, cells have been shown to sense and respond directly to the immediate nanotopography,[6,21–26] which means that the mode of cell settling on a given NS array is crucial for any application.

The two extremes of cell settling are illustrated in the scanning electron microscopy (SEM) images of **Figure 1**: A) A cell may stay suspended on top of the NSs like a tiny fakir or B) it may integrate completely into the array to the point where it contacts the flat substrate between the NSs. Only a few systematic experimental studies have been performed to describe these variations in the interface between NS arrays and cells[6,21,27] and thorough theoretical studies have focused on other aspects such as the deformation of a nonadherent cell around only a single NS[28] or the possible penetration of NSs through the cell membrane.[29]

Here, we further exploit a model assuming that cell settling on a NS array is governed by the balance between adhesion and the cost of membrane deformation[6] to systematically address this gap in our understanding of the interaction of cells with NSs. The cell settling has previously been suggested to depend

N. Buch-Månson, Dr. S. Bonde, Dr. T. Berthing, Prof. K. L. Martinez
Bionanotechnology and Nanomedicine Laboratory
Department of Chemistry and Nano-science Center
University of Copenhagen
Universitetsparken 5, DK-2100 Copenhagen, Denmark
E-mail: martinez@nano.ku.dk
Dr. J. Bolinsson, Prof. J. Nygård
Nano-science Center and Center for Quantum Devices
Niels Bohr Institute
University of Copenhagen
Universitetsparken 5, DK-2100 Copenhagen, Denmark

DOI: 10.1002/adfm.201500399

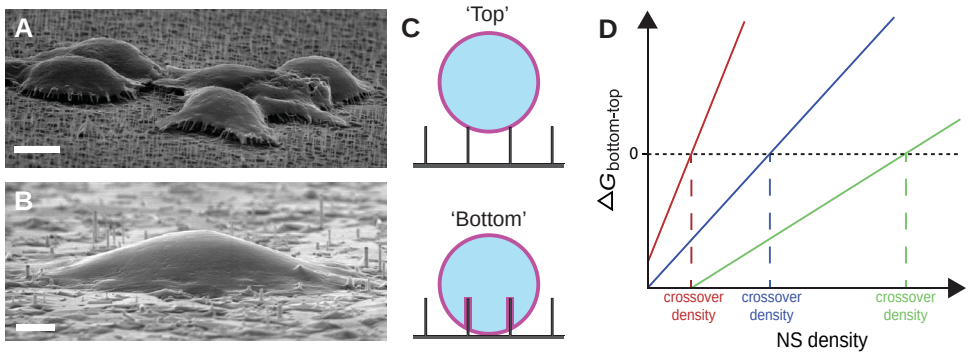

Figure 1. Predicting the mode of cell settling on NS arrays. A,B) SEM images of cells on different arrays reveal very different settling modes: A) The cells may stay suspended like tiny fakirs (Scale bar 5 μm) or B) they may integrate completely into the array (Scale bar 2 μm). C) Sketch of the two extreme cases of cell settling that are compared in the CINA model: A cell resting only at the very tips of the NSs ("Top") and a cell that has completely deformed around the NSs and contacts the flat substrate between them ("Bottom"). D) Sketch of $\Delta G_{\text{bottom–top}}$ as a function of NS density for three hypothetical sets of input values (r, l, w, σ, and κ). The steep red plot represents a system with a low crossover density, which implies that cells are likely to stay suspended ("Top" in C) on most densities. The green plot represents a system with a high crossover density, which implies that cells are likely to deform ("Bottom" in C), except on very high densities. The blue plot represents an intermediate scenario.

only on inter-NS spacing,[21] but here we evaluate also the influence of single NS features (diameter and length) and intrinsic cellular or interfacial parameters (cell bending modulus, cell surface tension, and specific adhesion energy) to establish generic predictive tools for any NS array or cell type. These findings should provide guidelines for a more rational design of NS arrays that are excellently adapted to any existing or future cellular applications.

2. Results and Discussion

2.1. Cell Interface with NS Arrays (CINA) Model

When modeling the complex behavior of a cell, it is useful to adopt a simplified view of the cell as being a homogenous and thin soft shell with some of the properties of the real cell collapsed into single average values. For such a soft shell, adherence and deformation on a surface is governed by the balance between different components of the free energy ΔG:

$$\Delta G = -w \cdot A_c + \sigma \cdot \Delta O + \Delta G_b \quad (1)$$

where w is the specific adhesion energy per unit area, A_c is the contact area between cell and surface, σ is the surface tension of the cell, ΔO is the increase in the surface area of the cell, and ΔG_b is the bending energy.[30]

For the specific case of the deformation of an initially spherical cell on an array of vertical NSs, two extreme cases are considered: a cell completely suspended on top of the NSs ("Top" in Figure 1C) and a cell deforming tightly around the NSs and settling completely into the array to the point where it contacts the flat substrate between NSs ("Bottom" in Figure 1C). We assume that the overall shape of the cell initially stays essentially the same at the two extremes, so that only the deformation around the NSs needs to be considered, and that the cell keeps its volume constant by unfolding more membrane as it deforms along the NSs (see S1, Supporting Information). We also take into account only the deformation of the basal plasma membrane and assume that the cell increases its apparent surface area by unfolding membrane wrinkles,[31] rather than by stretching the membrane. Furthermore, gravity will be ignored, as it is negligible compared with adhesive forces (see S2, Supporting Information).

In principle, NSs could also spontaneously penetrate through the plasma membrane, but numerous studies made by us and others on a wide variety of cell types, NS dimensions, materials and coatings have shown that under the influence of gravity alone, such penetration is a rare event at best.[7–9,13,27,32–34] Moreover, a recent theoretical study of the requirements for spontaneous penetration finds that it is only conceivable for a subset of NS array geometries and that the penetration will be a secondary event to initial cell settling,[29] which is the focus of the present model. In the cell interface with NS arrays (CINA) model, the NSs are therefore assumed to deform the membrane, rather than penetrating it.

Under these assumptions, the cost of transferring a cell from the "top" to the "bottom" state, $\Delta G_{\text{bottom–top}}$, is determined by the balance between the cost of forming the NS-induced membrane invaginations and the gain in cell-surface contact area at the NSs and flat substrate. For a NS shaped like a flat-ended cylinder with a cross-section radius r and length l, the geometrical quantities entering into $\Delta G_{\text{bottom–top}}$ are readily calculated for a projected cell area of 1 μm^2 and density x NSs μm^{-2} (see S3, Supporting Information) to give

$$\Delta G_{\text{bottom-top}} = -w(1\,\mu\text{m}^2 + x2\pi rl - x\pi r^2) + \sigma x2\pi rl + \kappa x\pi r^{-1}l \quad (2)$$

For densities corresponding to a negative value of $\Delta G_{\text{bottom–top}}$, deformation and settling into the NS array is predicted energetically favorable, whereas a positive value implies that deformation is unfavorable and the cell is predicted to rest on top of the NSs. The magnitude of $\Delta G_{\text{bottom–top}}$ will change depending on the actual projected cell area, but the prediction of when the value changes from negative to positive will not. The "crossover density" used in the following is defined as the exact NS density at which $\Delta G_{\text{bottom–top}} = 0$, i.e., the border between favorable deformation (NS densities below the crossover density) and

unfavorable deformation (NS densities above the crossover density).

Three hypothetical predictions are plotted in Figure 1D to illustrate that both the crossover density (where $\Delta G_{bottom-top} = 0$) and the steepness will change with different input values (r, l, w, σ, and κ). A low crossover density (red plot, Figure 1D) means that there is only a narrow low-density window to work with if cell deformation ("bottom" state) is crucial, whereas the window of densities appropriate for "top" settling is very wide. On the contrary, a high crossover density (green plot, Figure 1D) means that the density window for cell deformation is very wide and that "top" settling can only be achieved on very high densities. A steeper plot means that cell settling is more easily modulated by varying the NS density, whereas a more drastic change of density might be needed to effectively modulate cell settling for a shallow plot. For extreme combinations of input values, the slope of the plot may even be negative, which suggests that deformation is so favorable that the favorability of the "bottom" state increases with increasing NS density. This special case, if realistic at all, will not be considered here.

2.2. Influence of NS Array Dimensions—Theoretical Study

According to the developed CINA model, the parameters that may influence cell settling can be categorized as: () the purely geometrical features of the NS array (NS length, diameter, and density) and 2) the parameters partly or wholly related to the cell (w, σ, and κ). The geometrical properties of a NS array are typically better defined and controlled than the cell-related parameters, so the effect of varying NS length, diameter, and density will first be explored, while keeping the other parameters fixed to realistic values of $w = 2.2 \times 10^{-17}$ J μm^{-2},[35] $\sigma = 2.4 \times 10^{-17}$ J μm^{-2},[36] and $\kappa = 9 \times 10^{-19}$ J[37] that have been previously validated.[6] The effect of varying the cell-related parameters will then be evaluated in the second part of the paper.

In the CINA model, the cost of transferring the cell from "top" to "bottom" is evaluated at the level of the whole cell interfaced with the full nanotopography that an array of NSs constitutes. However, a deeper understanding of the effect of NS dimensions on cell settling requires a more detailed look at the deformation taking place at the single NS. For this purpose, the magnitude of the energetic contributions of a single NS-induced membrane invagination to each term (i.e., adhesion, tension, and bending) of $\Delta G_{bottom-top}$ (Equation (2)) and the overall energy (total) of the invagination have been plotted against NS diameter and length in **Figure 2**.

Comparing the plots in Figure 2A,B, it is found that the magnitudes of the adhesion and surface tension terms are close to equal, so that they nearly cancel each other out. Therefore, the bending term dominates the energy of the membrane invagination, which is clearly seen when comparing the plots in Figure 2C,D. The total energy only deviates slightly from the bending energy at higher diameters, where the magnitude of the bending term decreases and the small difference between the adhesion and surface tension terms therefore becomes important.

Thus, for the fixed set of w, σ, and κ used here, deformation around the single NS is never favorable, which means that there is an energy barrier to overcome if the cell is to be

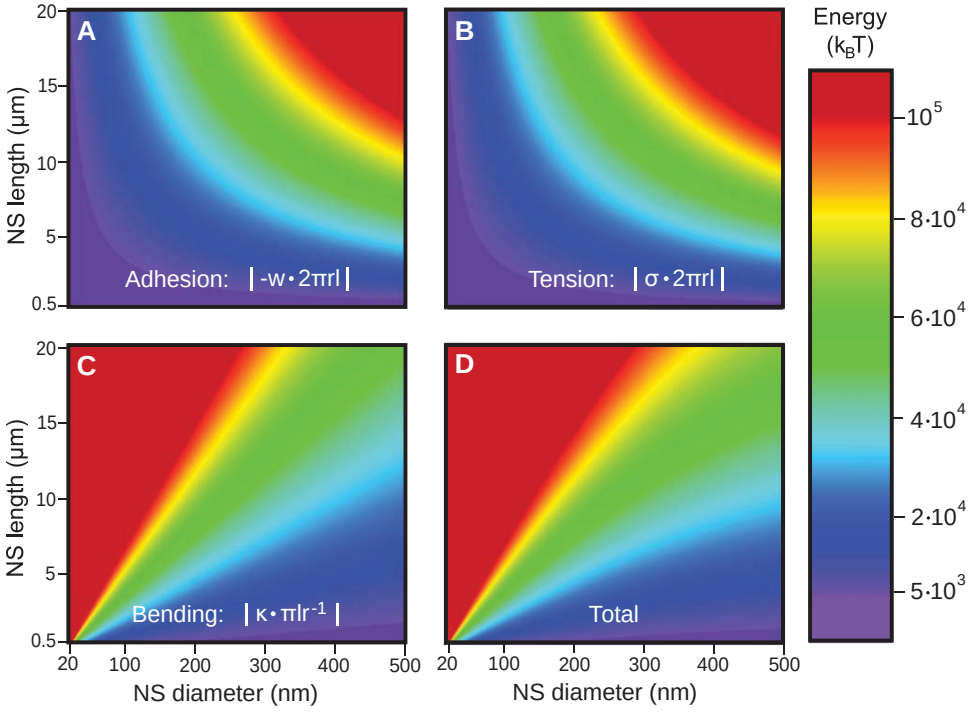

Figure 2. Energy of a single NS-induced membrane invagination. The magnitudes of the energetic contributions associated with A) adhesion, B) surface tension, and C) bending of the plasma membrane and D) the sum of the three terms have been plotted against NS length (l) and diameter ($2r$). w is the specific adhesion energy, σ is the surface tension, and κ is the bending modulus.

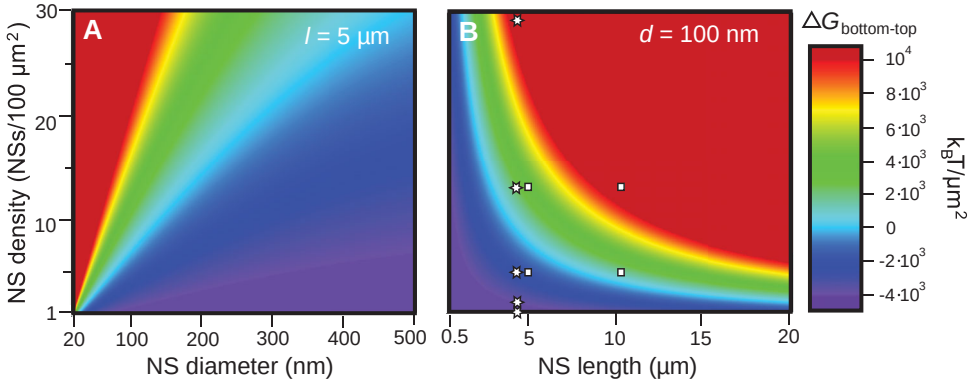

Figure 3. The dependence of $\Delta G_{bottom-top}$ on NS dimensions and density. The free energy difference between the "top" and "bottom" cell settling states per µm² projected cell area, $\Delta G_{bottom-top}$, has been plotted against both the NS density and A) diameter d or B) length l, while keeping l fixed to 5 µm or d fixed to 100 nm, respectively. Where $\Delta G_{bottom-top} < 0$, the "bottom" state is more favorable and where $\Delta G_{bottom-top} > 0$, the "top" state is more favorable. Where $\Delta G_{bottom-top} = 0$, which it is along the light blue trace, the two states are equally favorable. The square points marked in (B) correspond to the experimental conditions tested in Figure **5**, where $d = 100$ nm is kept constant, while the density and lengths are varied. The star-shaped points in (B) correspond to points tested in a previous study.[6]

transferred from the "top" to the "bottom" state (see Figure S4, Supporting Information). The initial deformation leading to the "bottom" state must therefore be driven by the favorable increase in adhesive contact at the flat substrate between NSs. However, partial cell deformation states in between the "top" and "bottom" extremes must be accounted for by later adaptations such as lipid redistribution, which could relax the tension of NS-induced invaginations, or stabilizing cytoskeletal remodeling.

To evaluate the effect of the geometry of a full array of NSs, the impact of both NS dimensions and density on the cost of cell deformation is explored in **Figure 3**, where the total free energy difference between a cell in the "bottom" state and a cell in the "top" state, $\Delta G_{bottom-top}$, is plotted against NS density and diameter (fixed length, l) (Figure 3A) or length (fixed diameter, d) (Figure 3B). In the regime where $\Delta G_{bottom-top} < 0$, the cells are more likely to deform into the NS array, and in the regime where $\Delta G_{bottom-top} > 0$, the cells are more likely to stay on top of the NSs. Along the trace where $\Delta G_{bottom-top} = 0$ (light blue), the corresponding density is the crossover density for the given set of d and l.

In accordance with the investigation of the energy at the level of the single NS-induced membrane invagination, the prediction for the whole cell is very sensitive to changes in NS dimensions. It can be seen that deformation soon becomes unfavorable even for just a few NSs per 100 µm², when $d < 50$ nm ($l = 5$ µm) or $l > 10$ µm ($d = 100$ nm) and that the energy changes rapidly with density for such dimensions. On the contrary, as the NSs get thicker or shorter, the density window for favorable deformation widens and the energy changes at a slower rate with density, so that one would have to move further away from the given crossover density to effectively move between the "top" and "bottom" regimes.

If instead the crossover density is plotted against both NS diameter and length as in **Figure 4**, a generic predictive tool emerges, where the density marking the border between the "bottom" and "top" regimes can be directly identified for any combination of d and l. Since the CINA model takes into account the local density of NSs, rather than the absolute inter-NS spacing, the predictions are valid both for ordered and random NS arrays. As expected from Figure 3, long and/or thin NSs correspond to low crossover densities, which means that on NSs of such dimensions, cells will tend to stay on top on most densities. On the contrary, short and/or thick NSs correspond to high crossover densities, which means that cells tend to deform on most densities. Owing to the dominance of the bending term (Figure 2), which is linear in l/r (Equation (2) and Equation S3.4, Supporting Information), these observations

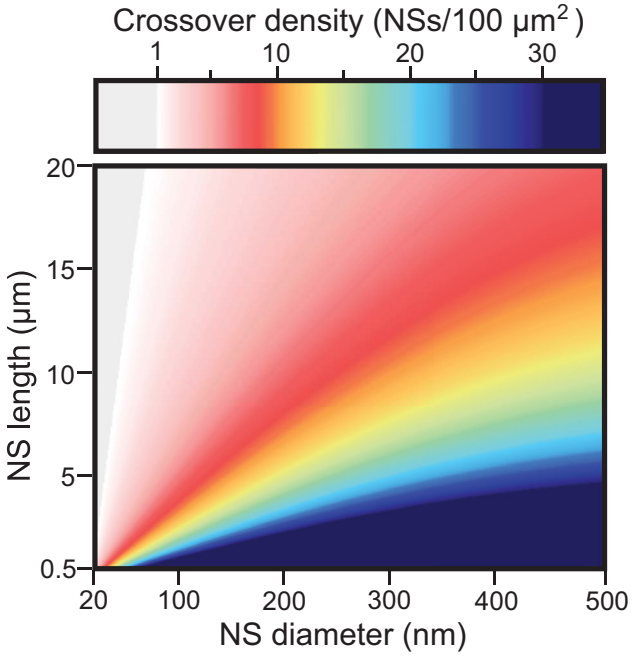

Figure 4. The dependence of the crossover density on NS dimensions. The crossover density, where $\Delta G_{bottom-top} = 0$, is plotted against NS diameter and length. Below the crossover density, $\Delta G_{bottom-top} < 0$ and cell deformation into the NS array is favorable. Above the crossover density, $\Delta G_{bottom-top} > 0$ meaning that cell deformation is unfavorable and the cells are predicted to stay on top of the NSs.

can be rephrased in terms of approximate NS aspect ratios ($l/2r = l/d$): For $l/d > 300$, the crossover density will be <1 NSs/100 μm^2, which essentially corresponds to having less than one NS per cell for most cell types; for $10 < l/d < 300$, the crossover density is found in the regime 1–30 NSs/100 μm^2, which approximately covers NS center-to-center spacings of 2–10 μm; for $l/d < 10$, the crossover density is >30 NSs/100 μm^2, which corresponds to very dense NS arrays.

Thus, NSs of higher aspect ratio are suitable for applications where cells are meant to stay suspended on top of the NSs, whereas NSs of lower aspect ratio are ideal for applications where cell deformation is key. Importantly though, changing the aspect ratio may change the geometrical stiffness of the individual NSs, which could alter the cell response.[21,22]

2.3. Influence of NS Array Dimensions—Experimental Study

To demonstrate how these findings may be utilized to understand and modulate cell settling in a real system, cells were interfaced with ordered vertical arrays of InAs NSs with different lengths (l = 5 and 11 μm) and densities (5, 13 NSs/100 μm^2), but a constant diameter of d = 100 nm. Although the CINA model does not assume that the NSs are positioned in an ordered array, the highly homogenous and well-defined nature of these NS arrays (see S5, Supporting Information) makes them ideal for experimental testing of the model, since the prediction is very sensitive to both the NS density, length, and diameter. Furthermore, we have previously shown with similar NS arrays that spontaneous penetration through the plasma membrane does not occur,[32] which validates the assumption of membrane deformation for this model system.

With a constant diameter of d = 100 nm, a length of l = 5 μm corresponds to a predicted crossover density of 7.7 NSs/100 μm^2, which is in between the two densities used (compare the leftmost square points in Figure 3B), whereas a crossover density of 3.5 NSs/100 μm^2, which is below both, is predicted for l = 11 μm (rightmost square points in Figure 3B). The distance between the cells and the flat substrate between the NSs was revealed by addition of an extracellular dye and measured from side views of the cells as shown in **Figure 5**A. In Figure 5C, the measured distances to the flat substrate between NSs in a non-treated array ("bare") have been plotted for the different lengths and densities. For l = 5 μm, most cells are slightly suspended above the surface (>1 μm) with 13 NSs/100 μm^2 and settle close to the surface (<1 μm) with 5 NSs/100 μm^2 as predicted. For l = 11 μm, the cells are suspended well above the surface at both densities as expected from the predicted low crossover density, but significantly further from the surface on 13 NSs/100 μm^2 than on 5 NSs/100 μm^2. This can be explained by consulting the plot of Figure 3B, where a change in density from 5 to 13 NSs/100 μm^2 corresponds to a dramatic change in $\Delta G_{bottom-top}$ of ≈12 000 k_BT μm^{-2} (i.e., from ≈2000 to ≈14 000 k_BT μm^{-2}) for 11-μm long NSs. These findings add to a previous successful prediction of cell settling where several points along the density axis were examined for a single NS length (l = 4.4 μm) and diameter (d ≈100 nm),[6] as also marked in Figure 3B (star-shaped points) and summarized in **Table 1** (cases 1 and 2).

In addition to the quantitative study above, the CINA model was also tested (assuming the same values for w, σ, and κ) to the best of our capacity against clearly reported cell settling in the literature. The first part of Table 1 ("Experimental data") summarizes the experimental details of each case (cell type, NS material, NS dimensions, and density) and whether the cell settling is found to be skewed toward "top" or "bottom" with these parameters. The last two columns ("CINA model") list the crossover density predicted from these parameters using the model (Figure S6, Supporting Information) and the corresponding predicted cell settling, i.e., if the predicted crossover density is below the density used in the study, the cells should be found in the "top" state, whereas the cells should be found

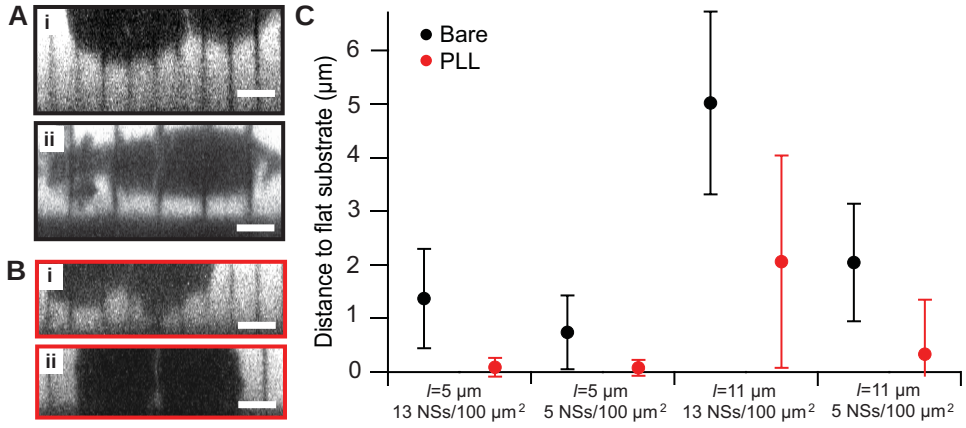

Figure 5. Experimental testing of the model. A,B) Examples of cell side views on 11-μm long A) bare or B) PLL-coated InAs NSs at densities i) 13 NSs/100 μm^2 or ii) 5 NSs/100 μm^2. The distance between the apical side of the cell and the flat substrate between the NSs is revealed by the addition of an extracellular dye, so that cells and NSs appear as shadows in a light background. The scale bars are 4 μm. C) Distances between cells and the flat substrate between NSs measured from side views as in (A,B) for different NS lengths (5, 11 μm) and densities (13, 5 NSs/100 μm^2, NS spacings 3 or 5 μm). The error bars are standard deviations based on measurements from on average 20 cells. The points collected on bare NSs are all significantly different ($p < 0.01$) between different NS densities and/or lengths, as are the points collected on PLL-coated NSs when compared with bare NSs of the same density and length.

Table 1. Summary of case studies from the literature where the observed mode of cell settling can be compared with the predictions of the model. Case numbers correspond to references: **1**,**2** = [6], **3** = [3], **4** = [11], **5**,**6** = [19], **7** = [25], **8** = [20], **9** = [7], **10**,**11** = [27], **12**,**13** = [21]. The cell-related parameters are fixed to $w = 2.2 \times 10^{-17}$ J μm^{-2}, $\sigma = 2.4 \times 10^{-17}$ J μm^{-2}, and $\kappa = 9 \times 10^{-19}$ J.

	Experimental data						CINA model	
Case	Cell type	Material	d [nm]	l [μm]	Density [NSs/100 μm^2]	Settling	Crossover density [NSs/100 μm^2]	Predicted settling
1	HEK293	InAs	92	4.4	1, 2, 5	Bottom	8	Bottom
2	HEK293	InAs	92	4.4	13, 29	Top	8	Top
3	Neurons	GaP	50	2.5	100[a)]	Top	8	Top
4	Fibroblasts	C[b)]	50	0.12	11 500[c)]	Top	161	Top
5	Mechanocytes	Si	140, 280	2–3	400	Top	18-49	Top
6	Cancer cells	Si	140, 280	2–3	400	Top	18-49	Top
7	Neurons	Si	70	0.7	300[a)]	Top	39	Top
8	Neurons	GaP	40, 80	2.5–5	115	Top	3–12	Top
9	CHO	Al_2O_3[b)]	250	1.5	20[a)]	Bottom	59	Bottom
10	Neurons	SiO_2	200	0.7	100	Bottom	103	Bottom
11	Neurons	SiO_2	500	0.7	100	Top	152	Bottom
12	Stem cells	Si	400	5	>25	Top	26	Top
13	Stem cells	Si	400	5	<25	Bottom	26	Bottom

[a)] Random array; [b)]Hollow NSs, which for simplicity are treated like solid structures; [c)]Approximated, since it is not provided.

in the "bottom" state if the predicted crossover density is higher than the actual density of the study.

The CINA model successfully predicts the "top" settling for cases 3–8, where the very high NS densities used are all far above the predicted crossover densities. It also correctly predicts the bottom settling in cases 9 and 10, where the NS densities are closer to the predicted crossover densities. However, in case 11, where a high NS diameter is combined with a very high NS density, the cells are found in the "top" state, although they are predicted to deform. In this extreme where the inter-NS gap also becomes very small, the cost of membrane deformation alone is probably insufficient to predict cell settling and case 11 may therefore mark the geometrical limits of the CINA model.

Among all the literature cases, the study by Bucaro et al. (cases 12 and 13) is particularly interesting, because it is the only study, aside from that of cases 1 and 2, where cell settling is systematically related to NS density. Here, a critical inter-NS spacing of ≈2 μm corresponding to a density of 25 NSs/100 μm^2 is found to mark the border between "top" and "bottom" settling. This is in excellent agreement with the CINA model where a theoretical crossover density of 26 NSs/100 μm^2 is found. In the study by Bucaro et al., the absolute inter-NS spacing, rather than the average density, is suggested to be the critical parameter, which would in turn suggest that the NS pattern is critical. The CINA model is not limited to ordered arrays or specific NS patterns, but this is a highly interesting aspect and the two theories might be complementary.

2.4. Influence of Cell-Related Parameters—Theoretical Study

Both the surface tension, σ, and the bending modulus, κ, are properties of the cell, whereas the specific adhesion energy, w, depends both on the cell and on the surface. The fixed set of σ, κ, and w values used in the simulations above were found in the literature and successfully predicted the settling of human embryonic kidney (HEK293) cells on an InAs NS array here and in a previous study[6] as well as cell settling in the literature. In this section of the paper, the potential effect of changing each parameter independently within a realistic range will be explored.

In **Figure 6**, this is done for different NS dimensions by fixing either the length l or the diameter d to typical values of 5 μm and 100 nm, respectively, while varying the other parameter. Other combinations of d and l can be found in Figure S7.1–3 (Supporting Information).

The apparent surface tension of cells arises from the contractile microfilaments of the cell cortex and their interaction with the plasma membrane.[31] The value of the surface tension, $\sigma = 2.4 \times 10^{-17}$ J μm^{-2}, used in the above simulations stems from micropipette aspiration measurements performed on a resting neutrophil,[36] but surface tensions of biological membranes cover the wide range of 10^{-18}–10^{-15} J μm^{-2}.[38] In Figure 6A,B, the effect of traversing this range is shown for different NS dimensions. For thinner NSs (d < 100 nm), changing the surface tension has only a modest impact on the predicted crossover density. This relative insensitivity is rooted in the fact that for thinner NSs, the surface area increase is vanishing, while the bending energy dominates (see Figure 2). On the contrary, for thicker NSs (d > 100 nm), the surface area increase is more considerable and the bending term is diminished, which causes the prediction to be very sensitive to changes in surface tension. Likewise, for shorter NSs, the bending term is decreased and the prediction becomes more sensitive to changes in surface tension.

The bending modulus of the cell membrane relates to the cell stiffness and is high for stiff cells and low for soft cells. The initial value taken for the bending modulus, $\kappa = 9 \times 10^{-19}$ J,

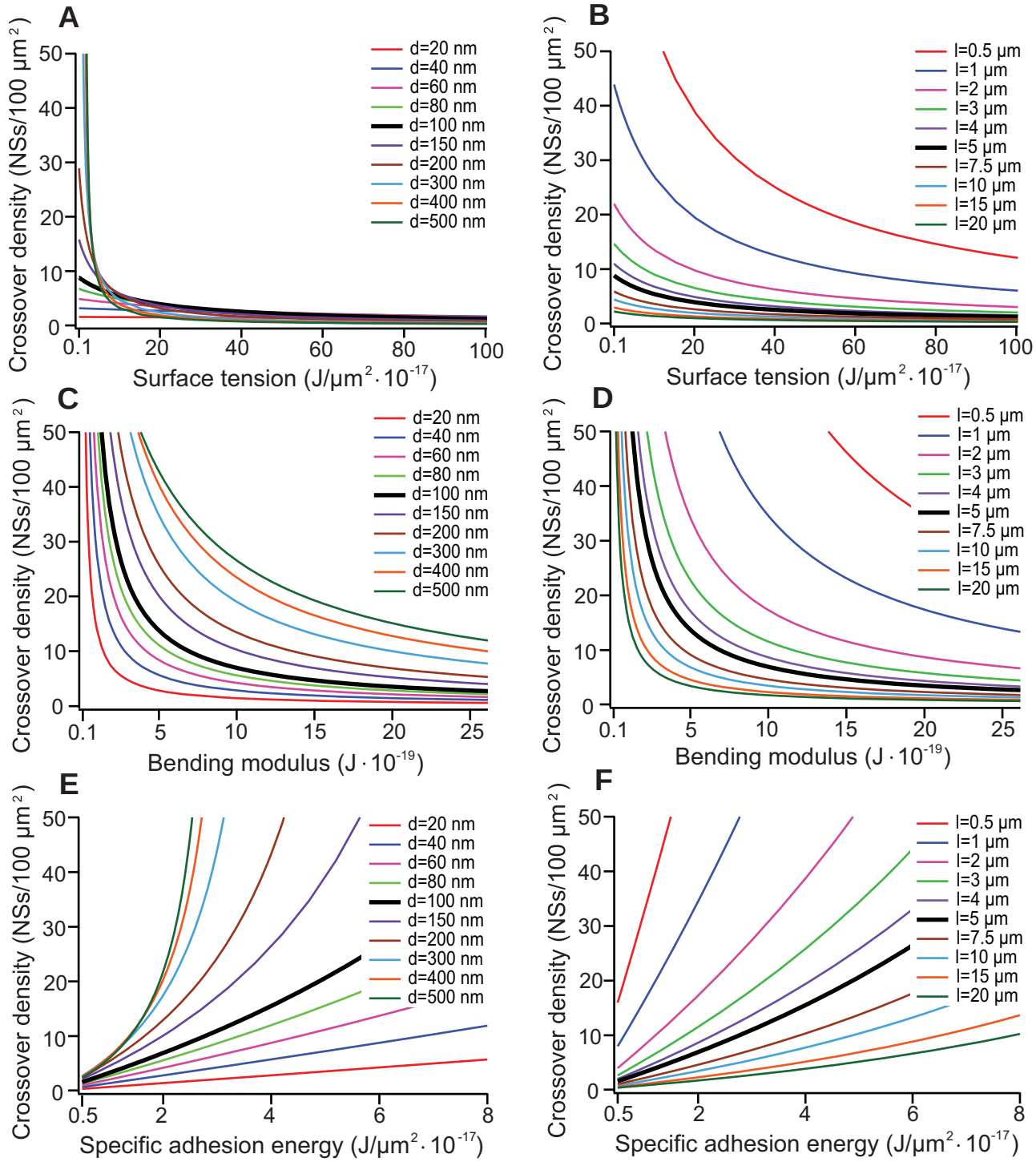

Figure 6. Effect on the predicted crossover density, when the A,B) surface tension, C,D) bending modulus, and E,F) specific adhesion energy are varied independently from the initial values of $\sigma = 2.4 \times 10^{-17}$ J μm^{-2}, $\kappa = 9 \times 10^{-19}$ J, and $w = 2.2 \times 10^{-17}$ J μm^{-2}, respectively, within a realistic range. The black lines are the tendencies for cell settling on NSs of dimensions $d = 100$ nm and $l = 5$ μm (as used in the cell settling experiments of Figure 5), while the colored lines give the tendencies when the A,C,E) NS diameter or B,D,F) NS length are independently varied (with l fixed to 5 μm or d fixed to 100 nm, respectively).

stems from membrane tether pulling experiments performed on a HEK293 cell,[37] but values on the order of 10^{-20}–10^{-18} J have been measured[39] and the effect of changes within this regime is presented in Figure 6C,D. As expected from the dominance of the bending term, the prediction is highly sensitive to changes in bending modulus over the whole range of

NS dimensions shown here. For high values of κ, the crossover density goes to low values, and for low values of κ, the crossover density goes quickly to high values. Thus, stiff cells are ideal for applications where "top" settling is desired, but if deformation is needed with such cells, the crossover density may be increased considerably by increasing the diameter and decreasing the length of the NSs. On the opposite, soft cells are ideal for applications where "bottom" settling is key, but the deformation probability may still be reduced significantly by changing to thinner and longer NSs.

The specific adhesion energy, which averages over many of the complicated interactions involved in cell adhesion onto a surface, will depend on both the cell type, the specific surface and even time. The starting value of the specific adhesion energy, $w = 2.2 \times 10^{-17}$ J μm^{-2}, stems from interference microscopy measurements performed on *Dictyostelium discoideum*[35] and falls close to values used in other models of cell settling.[29,40] However, the cell detachment energy may vary ≈fourfold for different surface coatings[41] and for vesicles, the change in specific adhesion energy can be as much as 30-fold.[42] In Figure 6E,F, the effect of varying the specific adhesion energy in the range 0.5×10^{-17}–8×10^{-17} J μm^{-2} is explored. As observed with the bending modulus, the specific adhesion energy is a potent parameter in modulating cell settling on a wide range of NS dimensions. However, the sensitivity decreases when going to very thin or long NSs, where the bending energy increases dramatically. According to the plots, strongly adhering cells will tend to deform on the NSs except if these are long and/or thin or the density very high, whereas less adherent cells will tend only to deform if the NSs are short and/or thick. If neither the cell type nor the NS array dimensions are negotiable, the specific adhesion energy can instead be modulated through surface coating.

In conclusion, the prediction is relatively insensitive to changes in surface tension over a wide range, except with short or thick NSs, and moderately or highly sensitive to changes in specific adhesion energy and bending modulus over the full range of NS dimensions considered here. Nevertheless, the predictions of the model were correct for a variety of cell types and NS materials, as seen from Table 1, although w, σ, and κ were kept fixed, which suggests that the initial values for these cell-related parameters are widely applicable. Where these initial values do not apply, Figure 6 provides a predictive tool for the direction and potency of the shift in the crossover density relative to the prediction of Figure 4.

2.5. Influence of Cell-Related Parameters—Experimental Study

To demonstrate experimentally that the specific adhesion energy w is a powerful modulator of cell settling, the effect of coating InAs NSs with the adhesion-promoting molecule poly-L-lysine (PLL) on cell settling was investigated for the same NS dimensions that were used in the experiment with bare NS arrays (Figure 5B,C, "PLL"). Comparing the behavior of cells on PLL-coated and bare arrays for $l = 5$ μm, it is seen that the crossover density shifts significantly above 13 NSs/100 μm^2 as a result of the PLL-coating, since for both densities, all cells are now found in the "bottom" state. For $l = 11$ μm, which would give a more shallow slope in Figure 6F (compare $l = 5$ with $l = 10$ μm), the increase in w by the same amount only brings the crossover density in between the two densities, so that cells can now deform completely on 5 NSs/100 μm^2, but remain largely suspended on 13 NSs/100 μm^2. Thus, the PLL coating have increased the specific adhesion energy by at least twofold—e.g., if w is increased from 2.2×10^{-17} to 5×10^{-17} J μm^{-2}, the crossover densities for $l = 5$ and $l = 11$ μm would be 21 and 9 NSs/100 μm^2, respectively, which fits the observations.

The fact that the cells are here shown to settle very differently when the spacing is kept constant, but the single-NS dimensions or the surface coating are altered, proves that NS spacing or density alone is insufficient to explain how cells settle into NS arrays. Furthermore, the successful explanation and prediction of phenomena observed >24 h following interfacing (Figure 5, Table 1) strongly suggests that the settling of the cell in the very initial phases of interfacing, where the present assumptions are most valid, is highly determinant of the long-term cell settling fate. Thus, the apparently simplistic view of the CINA model has proven a powerful one in expanding the understanding of the complex phenomenon of highly diverse cell settling on NS arrays.

3. Conclusion

By treating the cell as a simple soft shell, we have arrived at the CINA model, which allows for the extraction of generic concepts for the highly diverse settling of cells into different NS arrays. This phenomenon is important for many advanced cellular applications using NS arrays, but has hitherto not been approached systematically. The CINA model focuses on the balance between the cost of forming NS-induced membrane invaginations and the favorable gain in adhesive contact at the flat substrate between NSs and reveals that the cell settling is highly dependent on both single-NS dimensions and NS density. Thus, the cell settling state may be predicted from the dimensions of a given NS array, as demonstrated by applying the model to cases from the literature, or the cell settling may be effectively tuned by changing these parameters, as demonstrated experimentally. The CINA model is furthermore used to explore the effect of changing the cell-related parameters w, σ, and κ and it is shown how the potency of these are intimately related to and can be predicted from the single-NS dimensions. To corroborate these findings, it is demonstrated experimentally that the cell settling state can be tuned in a cell type-independent manner by changing the specific adhesion energy w through surface coating of different NS array geometries. The CINA model thus provides valuable guidelines for the rational design of NS arrays specifically suited for present and future applications where the mode of cell settling is paramount.

4. Experimental Section

NS Array Fabrication: As previously described,[4,32,43] electron beam lithography (EBL) was used to define regular patterns for the formation of Au particles or they were deposited randomly on InAs 111B wafers. The Au particles served as seeds for the epitaxial growth of arrays of

vertical InAs NSs using Molecular Beam Epitaxy (MBE). In the random arrays, NS densities were 7 or 220 NSs/100 μm^2, NS lengths were 1–5 μm and NS diameters were 70–200 nm. In the ordered arrays, NSs were positioned in hexagonal arrays with 3 or 5 μm spacing and the growth conditions were adjusted to yield NSs of different length (11 ± 2, 5 ± 1 μm) but with similar diameters of 100 ± 20 nm. SEM images of the ordered hexagonal NS arrays can be found in S5, Supporting Information.

Cell Culturing and Interfacing with NS Arrays: HEK293 cells (Sigma) were maintained at 37 °C, 5% CO_2, and >95% humidity in DMEM/F-12 Glutamax-I medium (Gibco) with 10% fetal bovine serum (FBS, Gibco), interfaced with NS arrays by drop-wise addition as previously described[4] and grown in DMEM with 10% FBS for 24 h prior to imaging.

SEM Imaging of Cells on NS Arrays: HEK293 cells grown on random NS arrays were fixed with glutaraldehyde and dehydrated with methanol as previously described.[4] The samples were then sputter coated with 5 nm Au and SEM images were collected using a JEOL JSM-6320F with 30 kV acceleration voltage.

Cell-Surface Proximity Study: Ordered hexagonal InAs NS arrays were either preincubated for 45 min with 0.1 mg mL^{-1} of PLL (Sigma) or left bare prior to interfacing with cells. HEK293 cells on these arrays were imaged in 100 × 10^{-6} M ATTO647 (ATTO Technology, Inc., New York, USA) with an inverted confocal microscope (Leica TCS SP5). The distance between the apical side of the cell and the flat substrate between NSs was measured using vertical cross sections through z-stacks of the confocal images ("side views") in ImageJ software. Approximately 20 cells from a single sample were analyzed per condition and the data from different conditions were compared using Student's unpaired *t* test with a two-tailed distribution where *p*-values <0.05 indicate statistically significant differences.

Supporting Information

Supporting Information is available from the Wiley Online Library or from the author.

Acknowledgements

The authors thank P. Fuerst, H. Haidara, and L. B. Oddershede for fruitful discussions and M. H. Madsen for technical support. For financial support, the authors thank the Danish Agency for Science Technology and Innovation (The Danish Council for Strategic Research—CLIPS and ANaCell projects, and The Danish Natural Science Research Council—FTP 11-116984) and the UNIK Synthetic Biology (funded by the Danish Ministry for Science, Technology and Innovation).

Received: January 30, 2015
Revised: March 19, 2015
Published online: April 15, 2015

[1] S. Bonde, N. Buch-Månson, K. R. Rostgaard, T. K. Andersen, T. Berthing, K. L. Martinez, *Nanotechnology* **2014**, *25*, 362001.
[2] K. R. Rostgaard, R. S. Frederiksen, Y.-C. C. Liu, T. Berthing, M. H. Madsen, J. Holm, J. Nygård, K. L. Martinez, *Nanoscale* **2013**, *5*, 10226.
[3] W. Hällström, T. Mårtensson, C. Prinz, P. Gustavsson, L. Montelius, L. Samuelson, M. Kanje, *Nano Lett.* **2007**, *7*, 2960.
[4] T. Berthing, S. Bonde, C. B. Sørensen, P. Utko, J. Nygård, K. L. Martinez, *Small* **2011**, *7*, 640.
[5] F. Mumm, K. M. Beckwith, S. Bonde, K. L. Martinez, P. Sikorski, *Small* **2013**, *9*, 263.
[6] S. Bonde, T. Berthing, M. H. Madsen, T. K. Andersen, N. Buch-Månson, L. Guo, X. Li, F. Badique, K. Anselme, J. Nygård, K. L. Martinez, *ACS Appl. Mater. Interfaces* **2013**, *5*, 10510.
[7] X. Xie, A. M. Xu, S. Leal-Ortiz, Y. Cao, C. C. Garner, N. A. Melosh, *ACS Nano* **2013**, *7*, 4351.
[8] Z. C. Lin, C. Xie, Y. Osakada, Y. Cui, B. Cui, *Nat. Commun.* **2014**, *5*, 3206.
[9] C. Xie, Z. Lin, L. Hanson, Y. Cui, B. Cui, *Nat. Nanotechnol.* **2012**, *7*, 185.
[10] J. T. Robinson, M. Jorgolli, A. K. Shalek, M.-H. Yoon, R. S. Gertner, H. Park, *Nat. Nanotechnol.* **2012**, *7*, 180.
[11] S. Park, Y.-S. Kim, W. B. Kim, S. Jon, *Nano Lett.* **2009**, *9*, 1325.
[12] E. Peer, A. Artzy-Schnirman, L. Gepstein, U. Sivan, *ACS Nano* **2012**, *6*, 4940.
[13] J. J. VanDersarl, A. M. Xu, N. A. Melosh, *Nano Lett.* **2012**, *12*, 3881.
[14] D. G. J. Mann, T. E. McKnight, J. T. McPherson, P. R. Hoyt, A. V. Melechko, M. L. Simpson, G. S. Sayler, *ACS Nano* **2008**, *2*, 69.
[15] A. K. Shalek, J. T. Gaublomme, L. Wang, N. Yosef, N. Chevrier, M. S. Andersen, J. T. Robinson, N. Pochet, D. Neuberg, R. S. Gertner, I. Amit, J. R. Brown, N. Hacohen, A. Regev, C. J. Wu, H. Park, *Nano Lett.* **2012**, *12*, 6498.
[16] M. S. Chan, P. K. Lo, *Small* **2014**, *10*, 1255.
[17] J. Pan, Z. Lyu, W. Jiang, H. Wang, Q. Liu, M. Tan, L. Yuan, H. Chen, *ACS Appl. Mater. Interfaces* **2014**, *6*, 14391.
[18] J. Peng, M. A. Garcia, J.-s. Choi, L. Zhao, K.-J. Chen, J. R. Bernstein, P. Peyda, Y.-S. Hsiao, K. W. Liu, W.-Y. Lin, A. D. Pyle, H. Wang, S. Hou, H.-R. Tseng, *ACS Nano* **2014**, *8*, 4621.
[19] Z. Li, J. Song, G. Mantini, M.-Y. Lu, H. Fang, C. Falconi, L.-J. Chen, Z. L. Wang, *Nano Lett.* **2009**, *9*, 3575.
[20] W. Hällström, M. Lexholm, D. B. Suyatin, G. Hammarin, D. Hessman, L. Samuelson, L. Montelius, M. Kanje, C. N. Prinz, *Nano Lett.* **2010**, *10*, 782.
[21] M. A. Bucaro, Y. Vasquez, B. D. Hatton, J. Aizenberg, *ACS Nano* **2012**, *6*, 6222.
[22] S.-W. Kuo, H.-I. Lin, J. H.-C. Ho, Y.-R. V. Shih, H.-F. Chen, T.-J. Yen, O. K. Lee, *Biomaterials* **2012**, *33*, 5013.
[23] J. Albuschies, V. Vogel, *Sci. Rep.* **2013**, *3*, 1658.
[24] Q. Ha, G. Yang, Z. Ao, D. Han, F. Niu, S. Wang, *Nanoscale* **2014**, *6*, 8318.
[25] G. Bugnicourt, J. Brocard, A. Nicolas, C. Villard, *Langmuir* **2014**, *30*, 4441.
[26] M. J. Dalby, N. Gadegaard, R. O. C. Oreffo, *Nat. Mater.* **2014**, *13*, 558.
[27] L. Hanson, Z. C. Lin, C. Xie, Y. Cui, B. Cui, *Nano Lett.* **2012**, *12*, 5815.
[28] P. Verma, I. Y. Wong, N. A. Melosh, *Biointerphases* **2010**, *5*, 37.
[29] X. Xie, A. M. Xu, M. R. Angle, N. Tayebi, P. Verma, N. A. Melosh, *Nano Lett.* **2013**, *13*, 6002.
[30] E. Sackmann, R. F. Bruinsma, *ChemPhysChem* **2002**, *3*, 262.
[31] T. Lecuit, P.-F. Lenne, *Nat. Rev. Mol. Cell. Biol.* **2007**, *8*, 633.
[32] T. Berthing, S. Bonde, K. R. Rostgaard, M. H. Madsen, C. B. Sørensen, J. Nygård, K. L. Martinez, *Nanotechnology* **2012**, *23*, 415102.
[33] A. M. Xu, A. Aalipour, S. Leal-Ortiz, A. H. Mekhdjian, X. Xie, A. R. Dunn, C. C. Garner, N. A. Melosh, *Nat. Commun.* **2014**, *5*, 3613.
[34] A. Aalipour, A. M. Xu, S. Leal-Ortiz, C. C. Garner, N. A. Melosh, *Langmuir* **2014**, *30*, 12362.

[35] R. Simson, E. Wallraff, J. Faix, J. Niewöhner, G. Gerisch, E. Sackmann, *Biophys. J.* **1998**, *74*, 514.
[36] D. Needham, R. M. Hochmuth, *Biophys. J.* **1992**, *61*, 1664.
[37] N. Khatibzadeh, S. Gupta, B. Farrell, W. E. Brownell, B. Anvari, *Soft Matter* **2012**, *8*, 8350.
[38] B. Pontes, N. B. Viana, L. T. Salgado, M. Farina, V. Moura Neto, H. M. Nussenzveig, *Biophys. J.* **2011**, *101*, 43.
[39] J. C. Neto, U. Agero, R. T. Gazzinelli, O. N. Mesquita, *Biophys. J.* **2006**, *91*, 1108.
[40] D. Cuvelier, M. Théry, Y.-S. Chu, S. Dufour, J.-P. Thiéry, M. Bornens, P. Nassoy, L. Mahadevan, *Curr. Biol.* **2007**, *17*, 694.
[41] A. Yamamoto, S. Mishima, N. Maruyama, M. Sumita, *J. Biomed. Mater. Res.* **2000**, *50*, 114.
[42] T. Gruhn, T. Franke, R. Dimova, R. Lipowsky, *Langmuir* **2007**, *23*, 5423.
[43] M. H. Madsen, P. Krogstrup, E. Johnson, S. Venkatesan, E. Mühlbauer, C. Scheu, C. B. Sørensen, J. Nygård, *J. Cryst. Growth* **2013**, *364*, 16.